

A Multi-Cloud Warm-Absorber Model for NGC 4051

M. Contini¹ and S.M. Viegas²

¹ School of Physics and Astronomy, Tel-Aviv University, Ramat-Aviv, Tel-Aviv, 69978, Israel

² Instituto Astronômico e Geofísico, USP, Av. Miguel Stefano, 4200,04301-904 São Paulo, Brazil

Running title : Warm-Absorber Model for NGC 4051

subject headings : galaxies : nuclei - galaxies : Seyfert - shock waves -
galaxies : individual : NGC 4051 - X-ray : galaxies

Abstract

A multi-cloud model is presented which explains the soft X-ray excess in NGC 4051 and, consistently, the optical line spectrum and the SED of the continuum. The clouds are heated and ionized by the photoionizing flux from the active center and by shocks. Diffuse radiation, partly absorbed throughout the clouds, nicely fits the bump in the soft X-ray domain, while bremsstrahlung radiation from the gaseous clouds contribute to the fit of the continuum SED. Debris of high density fragmented clouds are necessary to explain the absorption oxygen throats observed at 0.87 and 0.74 keV. The debris are heated by shocks of about 200-300 km s⁻¹. Low velocity (≤ 100 km s⁻¹) - density (100 cm⁻³) clouds contribute to the line and continuum spectra, as well as high velocity (1000 km s⁻¹) - density (8000 cm⁻³) clouds which are revealed by the FWHM of the line profiles. The SED in the IR is explained by reradiation of dust, however, the dust-to-gas ratio is not particularly high ($\leq 3 \times 10^{-15}$). Radio emission is well fitted by synchrotron radiation created at the shock front by Fermi mechanism.

1. Introduction

NGC 4051 is a SAB galaxy at $z=0.0023$. It is classified as a Seyfert 1 galaxy, and is characterized by unusually narrow permitted lines, only moderately wider than the forbidden lines (Osterbrock 1977).

Simultaneous observations by ROSAT-IUE and GINGA of a sample of 8 Seyfert 1 galaxies (Walter et al 1994), including NGC 4051, show that the UV to X-ray spectral energy distribution (SED) can be decomposed into two major distinct components: a nonthermal hard X-ray continuum and a broad emission excess (bump) spanning from UV to soft X-rays. All models (power-law, thin disk, bremsstrahlung, black body) are able to reproduce the soft X-ray spectra in the Walter et al. sample, except the power-law model for NGC 4051. The evidence that the power-law model is not a good representation of the X-ray spectrum of NGC 4051, when the absorbing column density is fixed to the galactic value, contrasts with the long established situation that the power-law is the best *simple* fit to X-spectra of active galactic nuclei (AGN). This indicates that the spectrum is more complicated, and, for example, could be affected by intrinsic absorption. The addition of a soft component to the X-ray spectrum, which accounts for an excess in the 0.1-2 keV band, is also raised by Fiore et al. (1992). From the study of GINGA data they found a spectral variability consistent with a constant underlying power-law slope modified by partial covering or by a 'warm absorber'.

On the other hand, the soft excess frequently found in EXOSAT spectra were formerly interpreted as thermal emission from the innermost regions of a viscous heated accretion disk (Arnaud et al. 1985). As suggested by Pounds et al. (1994), both the soft excess and the blue bump emission may arise, instead, from reprocessing the hard X-rays in dense cold cloudlets surviving close to the central source. The ionizing photons absorbed in optically thick material will be reemitted at the black-body equilibrium temperature ($10^5 - 10^6$ K) as long as the density of the absorbing gas is sufficiently high. Maximum temperatures of the bump component are evaluated to about 5×10^5 K (Walter et al. 1994).

Variability on small scale of NGC 4051 is used to reveal the characteristics of the emitting clouds and of the velocity field. The observed spectral variability on scale of hours can be explained in terms of a change in ionization parameter plus an emerging soft excess (Pounds et al. 1994). The assumption of a typical variability time scale of one hour leads to a matter density of $\geq 5 \times 10^7 \text{ cm}^{-3}$ and a thickness of the photoionized gas of $\leq 1.4 \times 10^{14}$

cm. Considering that the radius of the source of the optical and UV continuum is larger than a few 10^{14} cm, Walter et al. (1994) claim that it can be covered in less than 3 years if the velocity of the absorbing clouds is larger than 200 km s^{-1} .

From the spectral observations in the optical range (De Robertis & Osterbrock 1984) it appears that there may not be a simple dichotomy between the broad line region (BLR) and the narrow line region (NLR) in NGC 4051. Instead, the continuum of line widths suggests that the emitting regions may be inhomogeneously filled with clouds or filaments showing densities in a very large range, so that the division into a BLR and a NLR is an extreme simplification. The asymmetry of the narrow-line profiles is consistent with radial outflow or expansion of the gas. The presence of strong blue wings (Veilleux 1991) favors models with radial motion and a source of obscuration. NGC 4051 is peculiar also because its UV spectrum is very steep and probably affected by intrinsic reddening. The presence of dust in the nucleus of NGC 4051 has been suggested by several groups (Walter et al 1994). Veilleux (1991) claims that dust is probably present and is the source of line asymmetry and that the differences in profiles of $H\beta$ and $H\alpha$ are due to reddening and/or optical depth effects. Balmer fluxes are known to vary over periods shorter than one year.

The basic model of a warm absorber (Pounds et al. 1994) consists of a gaseous region close to the BLR photoionized by the central radiation, originating absorption features in the central X-ray radiation. This radiation is represented by a power-law characterized by a photon index and normalized by the intensity at 1 keV ($\text{photons cm}^{-2}\text{s}^{-1}\text{keV}^{-1}$). The procedure is first to fit the power-law plus a cold absorbing column. Then, add one or more components seeking the best fit. The warm absorber model introduces two free parameters: the column density, N , and the ionization parameter, U . Principal absorption edges are identified with ionized carbon, nitrogen, and oxygen. The effect of a warm absorber can be interpreted also as a set of emission features.

Komossa & Fink (1997) have recently modeled the absorbed spectrum of NGC 4051 from ROSAT observations in terms of warm absorption. Their excellent model can explain most of the features observed in the X-ray spectrum. However, some discrepancies with a general scenario still appear, e.g., reduced solar abundances are in contrast with the absence of dust, a single component warm absorber is in contrast with the plurality of cloud conditions found by De Robertis & Osterbrock (1984).

In this work we consider NGC 4051 in the light of a multi-cloud model, as was found

appropriate also for other galaxies (e.g. the Circinus galaxy model by Contini, Prieto & Viegas 1998). The clouds move radially outward the galaxy. A composite model which consistently accounts for the effects of the radiation from the active center and of the shocks on the emitting clouds is adopted. Particularly, we suggest that the soft X-ray excess can be reproduced by reprocessed radiation (diffuse radiation) emitted from the hot slabs of gas after being partially absorbed by optically thick regions throughout the clouds. The consistency of the model is checked up by fitting both the SED of the continuum in a large frequency range and the emission lines.

In §2 the general model is described. In §3 the soft X-ray excess is modeled. The results of model calculations are compared with the observed continuum SED and the line spectrum in §4 and §5, respectively. Final remarks follow in §6.

2. The model

Clouds in the NLR with different physical conditions and with radial outward motion are assumed by the model. A shock forms on the outer edge of the clouds while the power-law radiation from the active center (a.c.) reaches the inner edge. The flux from the central source and the shock are the primary sources of ionization and heating of the gas. The cloud may be depicted as consisting of a large number of parallel slabs in which the conditions within any given increment are essentially uniform. The gas is ionized and originates a diffuse radiation field through recombination and lines. The intensity of the diffuse radiation depends on the source function which cannot be determined unless the ionization equilibrium is already known (Williams 1967). In the source function are therefore implicit the effects of collisional ionization. The role of diffuse secondary radiation in shocked clouds is illustrated by Viegas, Contini & Contini (1998). Diffuse radiation which emerges from the heated slabs is partially absorbed throughout the cloud. We suggest that the soft X-ray excess may be produced by the reprocessed radiation, e.g. diffuse radiation, emitted from a group of clouds in different physical conditions.

The SUMA code is adopted (Viegas & Contini 1994 and references therein). A composite ionizing spectrum with spectral index $\alpha_{UV} = 1.4$ and $\alpha_X = 0.4$ is assumed for all models as for previous modeling (see Contini, Prieto, & Viegas 1998). The other input parameters, i.e., the shock velocity, V_s , the preshock density, n_0 , the radiation flux intensity

at 1 Ryd, F_ν (in number of photon $\text{cm}^{-2} \text{s}^{-1} \text{eV}^{-1}$), and the dust-to-gas ratio by number, d/g , are chosen from the observational evidence and are adjusted by the modeling. Cosmic abundances are assumed (Allen 1973) and the preshock magnetic field $B_0 = 10^{-4}$ gauss.

3. The soft X-ray excess

The observational data are taken from Komossa & Fink (1997, Fig. 5). We assume that many clouds, at different physical conditions, contribute to the 'warm absorption'. A large range of densities is considered. Actually, a continuum distribution of densities could be present. Velocities are in agreement with the observed emission line FWHM (De Robertis & Osterbrock 1974, Veilleux 1991). Some clouds are shock dominated, other are radiation dominated with radiation intensities in the range usually found for the NLR of Seyfert galaxies. The input parameters of the models used to fit the X-ray excess are listed in Table 1. The best fit of the X-ray excess by model calculations is shown in Figure 1. Models 12, 13, and 14 are not included in the figure and will be discussed further on. Each model represents one type of cloud with a characteristic geometrical width, D , which is also given in Table 1. Shock dominated (SD) models are calculated adopting $F_\nu = 0$. Notice that model 8 is a SD model corresponding to the radiation dominated (RD) model 9. For each model, the diffuse radiation emitted by each cloud is calculated. The thick solid line in Fig. 1 represent the weighted summed spectrum from the models. In the last column of Table 1 the weights, W , adopted for single-cloud models in the average sum are shown. The weights reflect the dilution factor $(r/d)^2$ (r is the distance from the clouds to the center and d is the distance to earth) and the covering factor. It can be noticed that an acceptable fit to the observations is obtained by the present sample of models, considering that the observed data are contaminated by residuals and errors.

X-ray data at energies higher than 1.3 KeV can be well fitted by the flat power-law radiation from the central source, which is directly reaching the observer. Lower energy photons are generally absorbed by the cloud. This can be easily seen in the curve representing model 5, which corresponds to high density clouds. The spectrum given by model 7 shows a trend similar to the observed one, however lacks the throats of absorption in the critical edges. The two primary flux models have the lowest weights.

High density clouds are invoked to fit the deep throat at about 0.85 KeV, which is

due to the O VIII edge. The geometrical thickness of the clouds are small, particularly for dense clouds, indicating that fragmentation is rather strong. This is consistent with a regime of turbulence in the presence of shocks. The weights of the high density models are very high, particularly for model 3. In the corresponding clouds the cooling rate is high, due to the high density; moreover, the hot gas emitting region is very small. Consequently, the flux emitted by each cloud is weak and many clouds are necessary to fit the data. This is consistent with the small D. Model 6 with a larger D has also a high weight. In this case most of the gas inside the cloud is cold and neutral because the intensity of the central radiation is relatively low.

Modeling implies the choice of a composite model which is seldom unique. The validity of the present composite model for the warm absorber will be checked in the next sections by the consistent fit to the observed continuum SED and to the line spectrum.

4. The continuum

References of the observed continuum below 10^{16} Hz are given in Table 2. Data in the X-ray range are from Komossa & Fink (1997).

The SED of the observed continuum is plotted in Fig. 2. Optical observations integrated over the whole galaxy are not included. For energies less than 13.6 eV, the continuum calculated by the models, which is essentially the sum of bremsstrahlung radiation emitted from the gas within the clouds, roughly fit the data. The weights adopted to sum up the models are the same as listed in Table 1. Reradiation by dust in the IR depends strongly on the shock velocity. The observed IR maximum constrains the dust-to-gas ratio (d/g value), while the frequency corresponding to the maximum depends on the dust temperature. The grains are heated by radiation and by collisions. Dust and gas mutual heating and cooling determine the temperature of dust which follows the temperature of the gas (Viegas & Contini 1994). For all the models dust-to-gas ratios in the range $1-3 \times 10^{-15}$ are adopted.

The SED of the continua corresponding to single models 1,2,3,4,6,8,9,10, and 11 (dotted lines) and their weighted sum (solid lines) are shown in Fig.2. The three components originating in the clouds (synchrotron emission due to Fermi mechanism, dust emission, and free-free emission) are shown separately.

It can be noticed that most of the models are below the lower edge of the figure because their weight is very low. The weighted sum corresponds to the SED of model 3 the weight of which largely prevails.

Depending on the models, the bremsstrahlung component peaks at a different frequency. So, the weighted average shows two peaks, one at $\sim 10^{14}$ Hz and another at 3×10^{16} Hz. Actually, absorption by ISM peaks at 3×10^{16} Hz (Zombeck 1990). In the radio range ($< 10^{10}$ Hz), the free-free emission is higher than the observational data, which are nicely fitted by synchrotron emission due to Fermi mechanism at the shock front. As happens for Circinus, the bremsstrahlung emission at such low frequencies is probably absorbed. In fact, if we assume an average temperature for the clouds of about 10^4 K, the optical depth for free-free absorption is greater than unity for $\nu \leq 10^{11}$, increasing at lower frequencies.

Notice, however, that the observed optical continuum is not well fitted yet. Moreover, reradiation by dust calculated by the models peaks at 10^{13} Hz, while the data peaks at $\sim 3 \times 10^{12}$ Hz. Therefore, the ensemble of clouds which explain the X-ray data is not complete, and models representing other clouds at different physical conditions must be included in the multi-cloud model. A final choice of the best fitting models will be possible after discussing the line spectrum. In fact, modeling the line and continuum spectra simultaneously implies cross checking of one another until a fine tuning of the models is obtained.

5. The optical - near-UV line spectrum

The observed line spectrum is taken from Malkan (1986, Table 1). A typing error crept in the published data has been corrected ($H\beta = 31$. and not 3.1, M. Malkan, private communication). The data are reddening corrected adopting $E(B-V) = 0.32$ which represent the obscuration inside the clouds (Malkan 1986). This is higher than the intrinsic reddening, $E(B-V)=0.08$ and galactic reddening $E(B-V)=0.02$. Notice that Walter et al. (1994) obtain $E(B-V)=0.05-0.13$.

The calculated line intensities relative to $H\beta$ are compared to the observations in Table 3. Radiation dominated models provide relatively high $HeII/H\beta$ (e.g. model 9), while shock dominated models provide higher $[OII]/H\beta$ and $[OIII]4363/H\beta$ (e.g. model 8). The results presented in Table 3 indicate that both radiation-dominated and shock-dominated clouds

should be taken into account for the final multi-cloud model. Model AV0 corresponds to the weighted average of the single-cloud models accounting for the X-ray data. This average model gives line ratios practically identical to model 3, which, in fact, largely prevails. However, the fit to the observed line ratios is not good enough. Therefore, models 12, 13, and 14, which are negligible in the fit of the soft X-ray excess, are invoked to improve the fit of the line ratios observed in the optical-near UV range.

The most noticeable features in the spectrum of NGC 4051 are that the ratio of the high ionization line widths to the low ionization line widths is considerably smaller than for other objects in the sample of De Robertis & Osterbrock (1984) and that blue wings up to -800 km s^{-1} are present in all the forbidden line profiles (Veilleux 1991). Veilleux (1991) also noticed four 'shoulders' (at -40 , -110 , -180 , and -350 km s^{-1}) in the observed line profiles. The line intensity ratios observed by Veilleux are not included in Table 3 which shows the line ratios to $\text{H}\beta$. In fact, the narrow and broad component of $\text{H}\beta$ could not be deblended.

The 'shoulders' indicate the velocities of emitting clouds which are represented by models 14, 13, 3, in addition to those represented by models 4 to 10. Model 12 represents the high velocity gas. The preshock density is high enough to cause the rapid cooling of the gas downstream. So, low ionization line ratios relative to $\text{H}\beta$ are particularly high (Table 3), and bremsstrahlung emission in the X-ray domain is low (Fig. 3). Dust reemission is completely annihilated by the sputtering of the grains in the immediate postshock region. Model 13 is characterized by a low V_s (100 km s^{-1}), a low n_0 (100 cm^{-3}), and a low primary flux ($F_\nu = 5 \cdot 10^{10}$ units). These conditions generally represent the clouds either in the outer NLR or in Liners (Contini 1997). This model shows a too high $[\text{OIII}] 4959/[\text{OII}] 3727$ line ratio, while model 14, which is a SD model characterized by a low V_s (50 km s^{-1}), provides a very strong $[\text{OII}]/\text{H}\beta$. The averaged spectrum (AV1) is given in the last column of Table 3 and shows an acceptable fit to the observations.

The relative contributions of models 3,12,13 and 14 to single line fluxes are shown in Table 4. As the models are distinguished particularly by the shock velocities, the results refer to the line profile features observed by Veilleux (1991). Model 3 is chosen to represent the contribution of the clouds generating the X-ray excess. Interestingly, the shock velocities adopted to fit the spectra confirm the observed prevailing FWHM of about $200\text{-}300 \text{ km s}^{-1}$ in the observed line profiles of $\text{H}\beta$, $[\text{OIII}] 4363$, and $[\text{OI}]$. Models calculated with $V_s = 100 \text{ km s}^{-1}$ provide 98-99 % of the $[\text{OIII}] 4959+5007$ and $\text{HeII} 4686$ lines, 94 % of $\text{He II} 3200$,

and 85-86 % of the [NeV] 3426 and [NeIII] 3869 lines, respectively. Models calculated with $V_s = 50 \text{ km s}^{-1}$ contribute essentially to the [OII], [NII], and [SII] 6717,6730 lines. The high velocity model (12) contributes to all the lines, except [OIII], [NeIII], [NeV], and HeII 4686. Model results are not in full agreement with observations for all the lines, but they roughly show how complex is the structure of the NLR which extends from the edge of the BLR to the outskirts of the galaxy.

Models 13 and 14 are chosen also to improve the fit of the continuum SED. In fact, the mutual heating of dust and gas provides a dust temperature low enough to settle the peak in the IR at about $3 \cdot 10^{12}$ Hz and the trend of model AV1 in the optical range improves the fit which was obtained by model AV0 (Fig. 3). Clouds corresponding to models 12, 13, and 14 contribute mostly to emission lines but not to the X-ray excess.

6. Final Remarks

Komossa & Fink find that the X-ray spectrum consists of a power-law modified by absorption edges and an additional soft excess during the high-state in source flux. Their results indicate a column density of ionized material of $\log N = 22.7$ and a ionization parameter of $\log U = 0.4$. The underlying power-law is in its steepest observed state with photon index $\Gamma_X = -2.3$. They assume that the absorber is one-component with a gas temperature of 3×10^5 K, metal abundances up to $0.2 \times$ solar, electron density $n_e \leq 3 \times 10^7 \text{ cm}^{-3}$, a thickness $D \geq 2 \times 10^{15} \text{ cm}$, at a distance $r \geq 3 \times 10^{16} \text{ cm}$ from the central power source, and no dust. Moreover, they claim that no emission line component can be fully identified with the warm absorber. Notice that in photoionization models, the high temperature is associated to a low chemical abundance. However, it is well known that the galaxies often show an abundance gradient, indicating higher abundances in the central regions. Thus unless the depletion is due to dust, it seems unreal to assume such low abundances in the central region of NGC 4051.

In the previous sections we have selected the models which consistently fit the observed continuum in all the frequency ranges and the line ratios. Our results show that the so-called warm absorber is composed by many clouds in different physical conditions. The column density within each cloud contributing to the soft X-ray excess does not exceed $5 \times 10^{20} \text{ cm}^{-2}$, considering a postshock compression of ~ 10 for low velocity clouds (200-300

km s⁻¹). Comparing with the results obtained by Komossa & Fink this indicates that hundreds of clouds form the warm absorber. The preshock densities span from the values which fit the NLR to values approaching those of the BLR, i.e. between 400 and 10⁷ cm⁻³, in agreement with the predictions of De Robertis & Osterbrock (1984) that a large range of densities characterize the emitting clouds in NGC 4051. Obviously, the clouds responsible of the edge absorption are the densest, in agreement with the density indicated by Komossa & Fink. Moreover, they predict no dust, while the modeling of the continuum in the present work shows that dust is present inside the clouds to explain the IR emission. However, the dust-to-gas ratio is rather low, even lower by a factor ≥ 3 than found for Liners by Viegas & Contini (1994).

The central radiation flux reaching the clouds ranges from 10¹¹ to 10¹³ photons per cm⁻² s⁻¹ eV⁻¹ at the Lyman limit which are "normal" values in the NLR of AGN (Viegas & Contini 1994). However, the high density clouds which explain the soft X-ray excess at ~ 1 keV are all shock dominated. This is an interesting result which shows that the gas is heated by the shock. Temperatures of about 6×10^5 K correspond in fact to shocks of ~ 200 km s⁻¹ . These temperatures are in agreement with the temperatures predicted by previous models (Komossa & Fink 1997 and references therein) which were explained by very strong radiation from the active center photoionizing and heating a gas characterized by low metal abundances, in order to reach such high temperatures. Our model shows that shock dominated clouds are present in large number, indicating that the central source radiation is screened, probably by the BLR clouds, and that the filling factor is high. Because the high temperature is due to shock, the fit to the observations is obtained with cosmic abundances.

Finally, in the present warm absorber model we assume that some very dense clouds are characterized by relatively low velocities (Table 1, models 1, 2, and 3). In the nuclear region of the Circinus galaxy some clouds characterized by velocities of 250 km s⁻¹ and preshock densities of 5000 cm⁻³ were invoked in order to fit the emission spectra (Contini et al. 1998). Generally, in AGN, higher densities correspond to higher velocities as for the clouds corresponding to model 12 ($n_0 = 8000$ cm⁻³, $V_s = 1000$ km s⁻¹). Notice that the high density low velocity clumps are characterized by a very small geometrical thickness in NGC 4051, therefore, they could be identified with the debris of high density-velocity clouds from the BLR edge which have been fragmented by cloud collision in a turbulent regime. Fragmentation is generally accompanied by a considerable loss of kinetic energy.

If model 3 represents these debris, their distance from the active center can be calculated from $F(\text{H}\beta)_{\text{obs}} d^2 = F(\text{H}\beta)_{\text{calc}} r^2$, where $\text{H}\beta_{\text{obs}}$ is the absolute flux of $\text{H}\beta$ observed at earth (Malkan 1994), d is the distance of the galaxy from earth ($d=14$ Mpc), $\text{H}\beta_{\text{calc}}$ is the absolute flux of $\text{H}\beta$ calculated at the gaseous clump, and r is the distance of the clumps from the active center. Adopting $\text{H}\beta_{\text{obs}} = 31. \times 10^{-14}$ erg cm $^{-2}$ s $^{-1}$ and $\text{H}\beta_{\text{calc}} = 27.$ erg cm $^{-2}$ s $^{-1}$ (see Table 3), r results 1.5 pc. The high density components of the warm absorber are thus located between the NLR and the BLR.

In conclusion, a multi-cloud model can explain the soft X-ray excess in NGC 4051, the optical emission line spectrum and the SED of the continuum. Indeed, modeling implies the choice of some conditions which should actually prevail. So single-cloud models must be considered as prototypes. The clouds are heated and ionized by the photoionizing flux from the active center and by the shocks. Due to the high temperature gas, diffuse radiation, partly absorbed throughout the clouds, is used to explain the bump in the soft X-ray domain, while free-free emission from lower temperature gas and dust reradiation from the ensemble of the clouds mainly fit the far IR to optical continuum. The fit of the continuum in the IR shows that the dust-to-gas ratio is not particularly high ($\leq 3 \times 10^{-15}$). Radio emission is well fitted by synchrotron radiation created at the shock front by Fermi mechanism. Debris of high density fragmented clouds are necessary to explain the absorption oxygen throats observed at 0.87 and 0.74 keV. The debris are heated by shocks of about 200-300 km s $^{-1}$. Low velocity (≤ 100 km s $^{-1}$) - density (100 cm $^{-3}$) clouds and high velocity (1000 km s $^{-1}$) - density (8000 cm $^{-3}$) clouds, which are revealed from the FWHM of the line profiles, contribute to the line and continuum spectra.

Acknowledgements. This paper was partially supported by the Brazilian funding agencies PRONEX/Finep, CNPq, and FAPESP.

References

- Allen, C.W. 1973 in "Astrophysical Quantities" (Athlon)
- Arnaud, K.A. et al. 1985, MNRAS, 217, 105
- Balzano, V.A., & Weedman, D.W. 1981, ApJ, 243, 756
- Contini, M. 1997, A&A, 323, 71
- Contini, M., Prieto, M.A., & Viegas, S.M. 1998, ApJ, 505, 621
- De Robertis, M.M. & Osterbrock, D.E. 1984, ApJ, 286, 171
- De Vaucouleurs, G., De Vaulcouleurs, A., Corwin, G.H.G. et al. 1991,
Third Reference Catalogue of Bright Galaxies, Version 3.9
- De Vaucouleurs, A., Longo, G., 1988, Catalogue of Visual and
Infrared Photometry of Galaxies from 0.5 μm to 10 μm (1961-1985)
- Fiore, F. et al. 1992, A&A, 262, 37
- Gregory, P.C. & Condon, J.J. 1991 ApJS, 75, 1011
- Ficarra, A., Grueff, G., & Tomasetti, G. 1985, A&AS, 59, 255
- Komossa, S. & Fink, H. 1997, A&A, 322, 719
- Lebofsky, M.J. & Rieke, G.H. 1979, ApJ, 229, 111
- McAlary, C.W., McLaren, R.A., & Crabtree, D.R. 1979, ApJ, 234, 471
- Malkan, M. 1986, ApJ, 310, 679
- Moshir, M. et al. 1990, Infrared Astronomical Satellite Catalogs, The
Faint Source Catalog, Version 2.0
- Osterbrock, D.E. 1977, ApJ, 215, 733
- Penston, M.V., Penston, M.J., Selmes, R. A., Becklin, E. E., &
Neugebauer, G. 1974, MNRAS, 169, 357
- Pounds, K.A., Nandra, K., Fink, H.H., & Makino, F. 1994, MNRAS,
267, 193

Rieke,G.H. 1978, ApJ, 226,550

Rieke,G.H. & Low, F.J. 1972, ApJL, 176,L95

Stein,W.A., & Weedman,D.W. 1976, ApJ,205,44

Soifer,B.T., Boehmer, L., Neugebauer, G., &Sanders, D. B. 1989, AJ,
98,766

Veilleux, S. 1991, ApJ, 369, 331

Viegas, S.M. & Contini, M. 1994, ApJ, 428, 113

Viegas, S.M., Contini, M., & Contini, T. 1998, A&A submitted

Walter, R. et al. 1994, A&A, 285, 119

Williams, R.E. 1967 ApJ, 147, 556

Wisniewski,W.Z. & Kleinmann,D.E. 1968, AJ,73,866

Zombeck, M.V. 1990 in "Handbook of Space Astronomy and
Astrophysics" Cambridge University Press, p. 199

Figure Captions

Fig. 1

The X-ray spectrum of NGC 4051. Filled squares indicate the data. Single model results are indicated by numbers which refer to Table 1. The thick solid line represents the weighted sum which best fits the data.

Fig. 2

The fit of the SED of the continuum by the ensemble of models which form the warm absorber. Dotted lines represent the single models and solid lines the weighted sum. Filled squares refer to observations in the X-ray (see Fig. 1). Open squares indicate the observation data at lower frequencies.

Fig. 3

Same as Fig. 2 including models 12 (dotted line), model 13 (short-dashed lines), and model 14 (long-dashed lines). The dot-dashed line shows that free-free emission is absorbed in the radio range. The thick solid lines refer to model AV1 and the thin solid lines to AV0.

Table 1
The input parameters of the models

model	n_0 (cm^{-3})	V_s (km s^{-1})	D (cm)	$\log(F_\nu)$ -	$\log(W)$ -
1	1.(6)	300	<4.5(13)	sd	-6.8
2	5.(5)	200	2.(12)	sd	-4.8
3	4.(5)	200	3.(13)	sd	+0.1
4	800	400	<2.(16)	sd	-10.4
5	800	420	5.(16)	12	-13.2
6	800	300	2.(17)	11	-6.9
7	600	300	1.(16)	11	-13.0
8	600	300	<1.(16)	sd	-9.4
9	600	300	1.(16)	11	-10.2
10	500	400	3.(16)	13	-10.7
11	400	200	7.(16)	12	-8.4
12	8000	1000	3.(17)	sd	-4.9
13	100	100	3.(16)	10.3	+4.0
14	100	50	<3(16)	sd	+3.8

Table 2
The data of the continuum

Wavelength	Frequency (Hz)	Reference
4400 Å	$6.81 \cdot 10^{14}$	1
5530 Å	$5.42 \cdot 10^{14}$	1, 2, 3
7000 Å	$4.28 \cdot 10^{14}$	2, 3
9000 Å	$3.33 \cdot 10^{14}$	2
1.23 μm	$2.44 \cdot 10^{14}$	4, 5
1.25 μm	$2.40 \cdot 10^{14}$	6
1.26 μm	$2.38 \cdot 10^{14}$	2
1.60 μm	$1.84 \cdot 10^{14}$	6, 7
1.66 μm	$1.81 \cdot 10^{14}$	4, 5
2.20 μm	$1.36 \cdot 10^{14}$	7
2.22 μm	$1.35 \cdot 10^{14}$	2, 3, 4, 5, 6
3.45 μm	$8.69 \cdot 10^{13}$	6
3.50 μm	$8.57 \cdot 10^{13}$	8, 9
3.54 μm	$8.47 \cdot 10^{13}$	3
3.65 μm	$8.21 \cdot 10^{13}$	4
4.65 μm	$6.45 \cdot 10^{13}$	4
5.00 μm	$6.00 \cdot 10^{13}$	9
10.5 μm	$2.86 \cdot 10^{13}$	9
10.6 μm	$2.83 \cdot 10^{13}$	6, 10
12.0 μm	$2.50 \cdot 10^{13}$	11, 12
21.0 μm	$1.43 \cdot 10^{13}$	10
25.0 μm	$1.20 \cdot 10^{13}$	11
60.0 μm	$5.00 \cdot 10^{12}$	11, 12
100.0 μm	$3.00 \cdot 10^{12}$	11, 12
6.18 cm	$4.85 \cdot 10^9$	13
73.5 cm	$4.08 \cdot 10^8$	14

1: De Vaucouleurs, G. et al. 1991 ; 2: Wisniewski, W.Z. & Kleinmann, D.E. 1968; 3: De Vaucouleurs, G. et al. 1988; 4: McAlary, C.W., McLaren, R.A., & Crabtree, D.R. 1979; 5: Balzano, V.A., & Weedman, D.W. 1981; 6: Rieke, G.H. 1978; 7: Penston, M.V. et al. 1974; 8: Stein, W.A., & Weedman, D.W. 1976; 9: Rieke, G.H. & Low, F.J. 1972; 10: Lebofsky, M.J. & Rieke, G.H. 1979; 11: Moshir, M. et al. 1990; 12: Soifer, B.T. et al. 1989; 13: Gregory, P.C. & Condon, J.J. 1991; 14: Ficarra, A., Grueff, G., & Tomasetti, G. 1985.

Table 3
The line spectra

	obs ¹	mod 1	mod 2	mod 3	mod 4	mod 6	mod 8	mod 9	mod 10	mod 11	mod AV0	mod 12	mod 13	mod 14	mod AV1
[OIII] 4959	0.45	1.5(-4)	0.019	0.013	0.18	0.14	3.5	7.7	0.06	3.6	0.013	2(-4)	2.5	0.075	0.76
HeII 4686	0.2	1.7(-3)	2.6(-3)	1.5(-3)	0.027	3.3(-4)	0.04	0.68	0.89	0.85	1.5(-3)	6(-6)	0.9	0.0	0.27
H _γ	0.40	0.46	0.45	0.45	0.45	0.45	0.43	0.47	0.47	0.47	0.45	0.45	0.45	0.45	0.46
[OIII] 4363	↑	3(-3)	0.15	0.08	0.06	1(-4)	0.44	0.35	0.01	0.27	0.08	4(-4)	0.14	0.014	0.09
[SII] 4072+	-	1.	0.09	0.06	0.47	0.05	0.48	1.2	0.0	1(-5)	0.06	1.2	2(-5)	0.87	0.16
[NeIII] 3869	0.25	0.025	0.085	0.05	0.36	7.3(-3)	1.32	4.4	0.014	0.8	0.05	3(-3)	0.74	0.05	0.26
[OII] 3727+	0.42	4(-4)	1(-3)	7(-4)	0.6	0.046	3.7	0.04	0.0	0.023	7(-4)	0.16	0.11	120.	0.5
[NeV] 3426+	0.59	0.01	0.3	0.17	0.34	9(-5)	2.65	0.05	9.3	6.17	0.17	1(-6)	2.24	0.0	0.79
HeII 3204	0.1	8(-4)	2(-3)	1.1(-3)	0.014	1.2(-4)	0.034	0.28	0.4	0.37	1.1(-3)	0.06	0.37	0.0	0.12
H β ²	-	1.6(3)	18.	27.	0.063	81.7	5(-3)	0.45	0.62	0.67	-	4(5)	1.2(-3)	2.5(-5)	-

¹ corrected ($E_{(B-V)}=0.32$)

² in $\text{erg cm}^{-2} \text{s}^{-1}$

Table 4

The % of the different components in single line fluxes

	mod	mod	mod	mod
	3	12	13	14
[SII] 6730	7.2	6.7	2.0	84.
[SII] 6717	2.64	2.4	1.7	93.
[NII] 6583	2.55	37.4	12.8	47.2
[OI] 6300+	92.2	6.4	0.0	1.37
[OIII] 4959	1.15	2.6(-3)	98.8	0.04
HeII 4686	0.37	7.4(-3)	99.6	0.0
[OIII] 4363	56.	0.04	43.7	0.057
[SII] 4072+	24.7	73.2	3.6(-3)	2.1
[NeIII] 3869	13.2	0.12	86.6	0.078
[OII] 3727+	0.089	3.0	6.0	90.7
[NeV] 3426+	14.6	0.0	85.4	0.0
HeII 3204	0.62	5.0	94.2	0.0
H β	62.6	9.27	27.8	0.37

Fig. 1

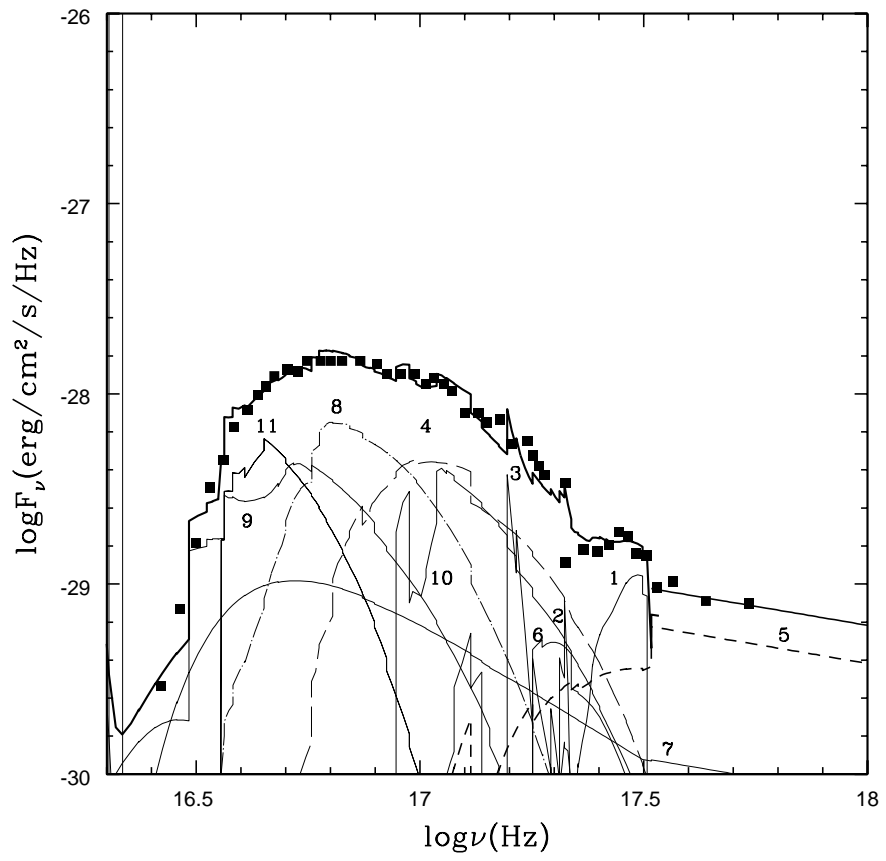


Fig. 2

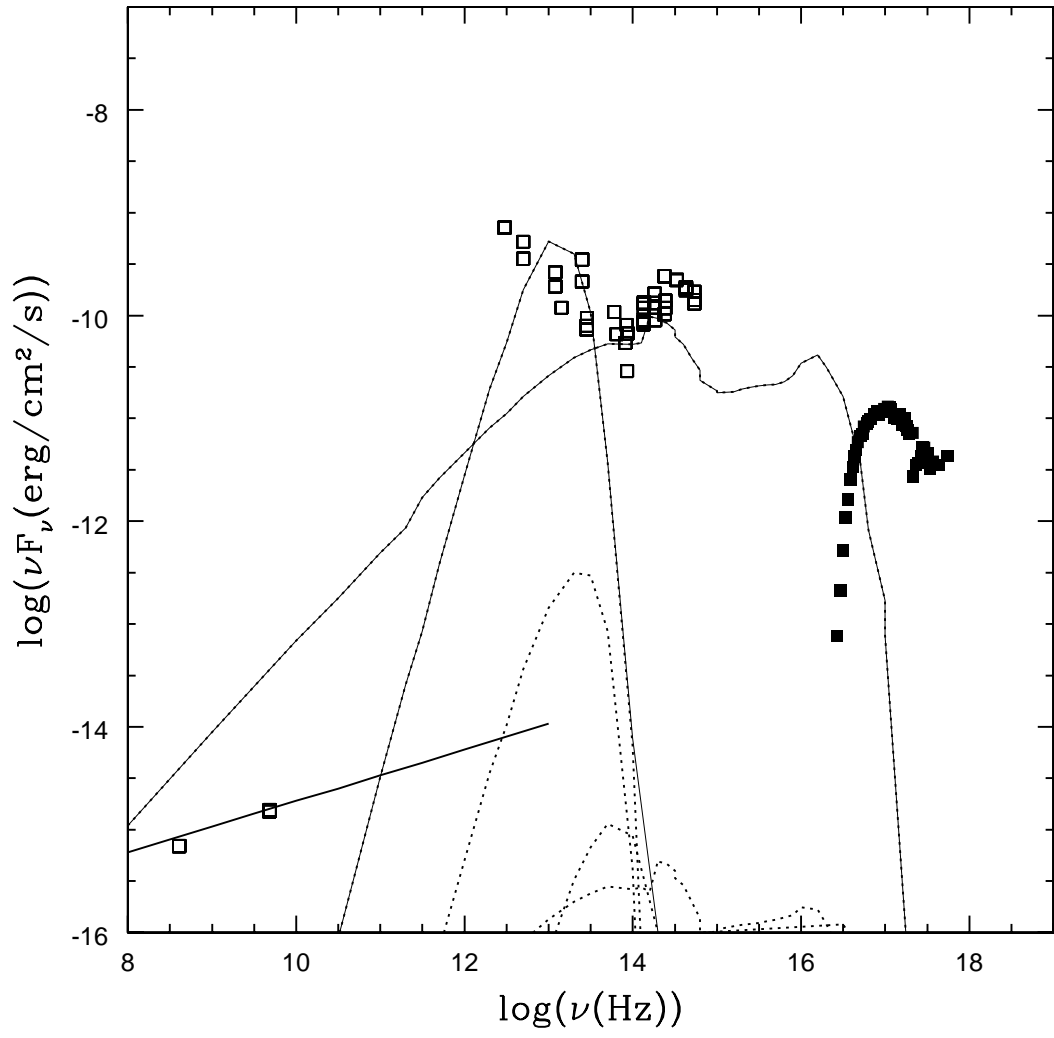


Fig. 3

